Kinetically-controlled low-temperature solid-state metathesis of manganese nitride Mn_3N_2

E. G. Rognerud,[a] C. L. Rom,[a] P. K. Todd,[a] N.R. Singstock,[b] C. J. Bartel,[b] A. M. Holder,[b,c] J. R. Neilson[a*]

[a] Department of Chemistry, Colorado State University; Fort Collins, CO USA 80523-1872

[b] Department of Chemical and Biological Engineering, University of Colorado; Boulder, CO 80309, USA

[c] National Renewable Energy Laboratory; Golden, CO 80401, USA

* james.neilson@colostate.edu

ABSTRACT

The synthesis of inorganic metal nitrides poses a challenge due to the low reactivity of N_2 gas at low temperatures, yet entropy driven formation of N_2 gas at high temperature. In contrast, synthetic approaches using more activated forms of nitrogen can be used to overcome the inertness of N_2, but increased exothermicity can also result in diminished stoichiometric control and the activation of deleterious competing pathways. Here, kinetically-controlled solid-state metathesis reactions are used to prepare Mn_3N_2 without the use of experimental conditions that increase the chemical potential of nitrogen and are known to produce phase impurity (e.g., NH_3, N_2-based plasma, azides, or high pressure). The solid-state metathesis reaction between $MnCl_2$ and Mg_2NCl or Mg_3N_2 is shown to generate Mn_3N_2, a phase on the border of stability. Highly exothermic control reactions performed with Li_3N, Ca_3N_2, and Ca_2NCl yield poorly crystalline, nitrogen-deficient Mn-N phases and N_2 formation. The reactions with Mg_2NCl and Mg_3N_2 do not self-propagate and have the lowest predicted free energies of reaction. A series of reactions performed at different times and temperatures, as well as *in situ* synchrotron X-ray diffraction, illustrate the importance of kinetic competence and implicates the mechanism for this competence: the formation of a solid-solution, $Mg_xMn_{1-x}Cl_2$, between the halide precursor ($MnCl_2$) and the halide product ($MgCl_2$) coupled to a mildly exothermic reaction. Kinetically-controlled solid-state metathesis continues to provide an avenue toward the synthesis of materials that cannot be prepared under traditional, high-temperature ceramic methods.

INTRODUCTION

Transition metal nitrides have developed considerable interest in fields such as ceramics, photovoltaics, and batteries because of their unique bonding patterns, high hardness, photoactive

band-gap and many more properties.[1,2] Unfortunately, the development of these materials is limited by their difficult synthesis. The formation of nitrogen gas is often a kinetic (at low temperatures) and entropic (at high temperatures) competitor to the formation of metal nitrides.[3] Activated nitrogen, as found with nitrogen plasmas ($N^{\bullet}$) or unstable molecules (N_3^-) has recently garnered success in the synthesis of new binary[2] and ternary[4,5] nitrides. However, the interdiffusion of nitride-containing precursors, as in solid-state metathesis (SSM),[6] offers new opportunities to synthesize metal nitrides. SSM reactions provide a low activation temperature alternative to the solid-state synthesis of many materials, which includes nitrides.[6–8] The SSM of metal nitrides has typically involved the combination of transition metal halides with alkali or alkaline earth nitrides. Many of these reactions are sufficiently exothermic as to be self-propagating (cf., 1300 °C for ZrN); however, upon self-heating, kinetic control may be lost and N_2(g) may be formed instead.[6,9]

Solid-state metathesis reactions need not be self-propagating due to the exothermic self-heating of the reaction. Our group has shown that solid-state metathesis reactions can be selected to enable kinetic control, as metastable products can be isolated from low-temperature, non-propagating reactions.[10–13] Furthermore, we recently recognized the role of kinetic competence in solid-state reactions, stipulating that the precursors have the necessary ability to perform the reaction at the given temperature, as it pertains to atomic transport and reactivity; this approach enables the synthesis of materials that are unstable at higher temperatures (e.g., orthorhombic $YMnO_{3+\delta}$)[14].

Manganese nitrides offer a platform for investigating controlled, stoichiometric nitride synthesis. At least four manganese nitride phases are known and include Mn_4N, Mn_2N, MnN (i.e., Mn_6N_{5+x}), and Mn_3N_2.[15,16] Of particular interest is the non-interstitial compound, Mn_3N_2, which has been sought after for catalysis[17] and high-temperature antiferromagnetism (T_N = 927 K).[16] While Mn_4N[18] can be prepared from reaction of Mn and N_2(g), and Mn_2N from reaction of Mn and NH_3(g),[19] compounds with increased nitrogen composition, such as Mn_3N_2 and Mn_6N_5, have required an increased chemical potential of nitrogen, as enabled by plasma-enhanced sputtering[20] or molecular beam epitaxy,[21] high pressure (N_2 or NH_3),[22] reaction with NaN_3,[16] and via $LiNH_2$ or $NaNH_2$ salt metathesis or flux.[23–25] In many of the reported syntheses for Mn_3N_2, decomposition products include Mn_4N or Mn_2N (with the necessary production of nitrogen

gas).[25] This contrasts the expected more thermodynamically favorable formation of "MnN" (Mn_6N_5) as a decomposition product based on the Mn-N phase diagram.[2,15]

This contribution describes how Mn_3N_2 is produced using kinetically-competent Mg-based reactions, 2 Mg_2NCl + 3 $MnCl_2$ → Mn_3N_2 + 4 $MgCl_2$ and Mg_3N_2 + 3 $MnCl_2$ → Mn_3N_2 + 3 $MgCl_2$. Synthesis at higher temperatures loses stoichiometric control, as Mn_2N (and presumably $N_2(g)$) forms. From reactions quenched at lower temperatures, as well as *in situ* X-ray diffraction, solid-solution behavior for $Mg_xMn_{1-x}Cl_2$ is observed, suggesting that this intermediate plays a role in enabling kinetic competence of the solid-state reaction. Control reactions with Li_3N, Ca_3N_2, and Ca_2NCl yield poorly crystalline, nitrogen-deficient Mn-N phases and N_2 formation; these control reactions are nearly twice as enthalpically favorable, and the halide salt by-products are known to not form solid-solutions with $MnCl_2$. By "turning down the heat,"[26] the solid-state metathesis reactions of 2 Mg_2NCl + 3 $MnCl_2$ and Mg_3N_2 + 3 $MnCl_2$ yield stoichiometrically-controlled reactions and formation of Mn_3N_2.

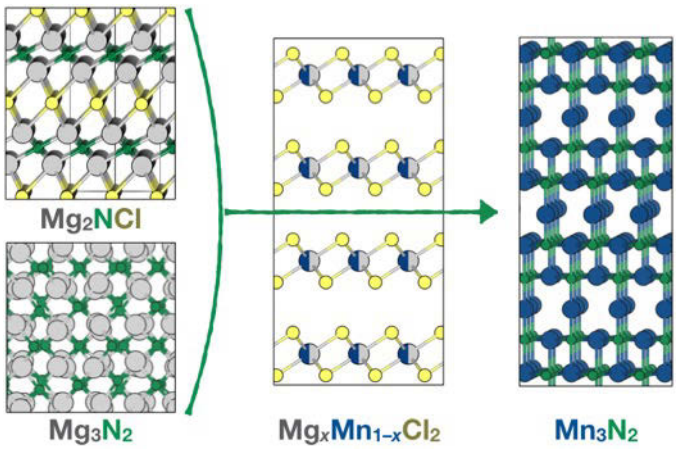

Figure 1: Schematic representation of the solid-state reaction pathway through the solid solution ($Mg_xMn_{1-x}Cl_2$) intermediate that plays a key role in enabling kinetic competence. Shown is the transformation of Mg_2NCl (top left) or Mg_3N_2 (bottom left) into Mn_3N_2 (right).

METHODS

All precursors were prepared and stored in an argon filled glove-box (O_2 < 0.1 ppm, H_2O < 0.5 ppm). Mg_2NCl was synthesized as previously reported with Mg_3N_2 (Alfa Aesar: 99% purity) and $MgCl_2$ (Sigma Aldrich: 98% purity).[27] Stoichiometric amounts of Mg_3N_2 and $MgCl_2$ were combined in an agate mortar and pestle and ground into a homogenous tan powder. The

powder was then pressed (P ~1 ton) into a dense pellet and placed in a quartz ampoule. This ampoule was then brought out of the glovebox and quickly sealed under vacuum (P < 10 mTorr) using an oxygen/methane torch. The sealed ampoule was then heated at 5 °C/min in a muffle furnace to a set point of 550 °C. The reaction was held at temperature for 7 days, and then allowed to cool to room temperature. The reactions reported here are sensitive to the precise temperature such that thermal gradients within the muffle furnaces influence reproducibility. Pelletized samples experienced temperatures approximately 20 to 40 °C below the temperature reported by the muffle furnace thermocouple, as probed by an external thermocouple. All temperatures reported are the nominal temperature set point, with estimates to the actual uncertainty described in the text.

The reactions of $MnCl_2$ (Alfa Aesar: 97% purity) with Mg_3N_2 or Mg_2NCl to produce Mn_3N_2 were performed under a similar procedure. Stoichiometric amounts of reactants were combined with $MnCl_2$ in an agate mortar and pestle resulting in a homogenous pink powder. This powder was then pressed into a pellet (P ~1 ton) and placed in a quartz glass ampoule within an inert glovebox. Out of the glovebox, the ampoule was quickly sealed under vacuum (P < 10 mTorr) with an oxygen/methane torch. Sealed ampoules were heated in a conventional muffle furnace for various heating schedules described in the text; all reactions were performed with a ramp rate of 1 °C/min and furnace cool.

Control reactions were run with Li_3N (Alfa Aesar: 99.4% purity), Ca_3N_2 (Alfa Aesar: 99% purity), and Ca_2NCl. Ca_2NCl was synthesized from $CaCl_2$ and Ca_3N_2 as previously reported.[28] The control reactions were performed under the same conditions as discussed above.

The products of all reactions were characterized by powder X-ray diffraction (PXRD) and Rietveld analysis. PXRD was performed using a Bruker DaVinci diffractometer with CuK_α X-ray radiation. All samples were prepared for PXRD from within the glove-box by placing powder on silicon wafers to reduce the background and covered in Kapton® tape to prevent exposure to the atmosphere. Some PXRD samples were prepared for quantitative Rietveld analyses by grinding known masses of silicon powder (as an internal standard) with known masses of the sample. Rietveld analyses were performed using the software TOPAS v6 (Bruker AXS) to obtain values for cell parameters, occupancies, and phase fractions.

In situ PXRD studies were conducted at 17-BM-B of the Advanced Photon Source at Argonne National Lab (λ = 0.24125 Å). Precursors were packed in extruded borosilicate

capillaries and flame sealed under vacuum (<10 mTorr). The tip of a thermocouple was placed against the capillary, within 3 mm of the X-ray beam, and two parallel resistive heaters controlled the sample temperature during the measurements with much greater accuracy than the muffle furnaces. Data collection was carried out with a 2048 × 2048 PerkinElmer 2D plate detector at a distance of 70 cm from the sample. The 2D diffraction patterns were then radially integrated with GSAS-II.[29] Sequential Rietveld refinements were conducted using TOPAS v6 (Bruker AXS) to identify phase fraction, the occupancy (x) of $Mg_xMn_{1-x}Cl_2$ and lattice parameters. Strain was also refined. The Mn_2N phase was only refined for the dwell scans to prevent poor convergence of the calculation, although small peaks can be qualitatively observed for data collected above T = 385 °C.

The thermochemistry of manganese nitride stability and metathesis reaction energetics were computationally evaluated at finite temperatures using quantum chemical calculations. All atomic structure and total energy calculations were performed using the projector augmented-wave method within the VASP code,[30,31] and in accordance with our previous calculation parameters used for computing binary nitride phase diagrams and evaluating stability.[2] In brief, the Perdew-Burke-Ernzerhof (PBE) generalized gradient approximation exchange-correlation functional[32] was employed for all calculations, with a plane-wave energy cutoff of 520 eV, and Γ-centered Monkhorst-Pack k-point grid. The energy cutoff, *k*-point density, and related convergence settings were sufficient to achieve total energy convergence of < 0.5 meV/atom for all calculations.[2] These computational parameters were selected to enable the direct evaluation of thermodynamic stability and reactions energetics involving all potential competing compounds and formation enthalpies computed within this work and those reported within the Materials Project database.[33] We note that our predicted Mn-N convex hull phase diagram is consistent with the results reported using the meta-GGA SCAN functional and elemental reference energy correction schemes for evaluating thermochemistry[2] to well within the error bars of these methods,[34] yet there is a discrepancy between these methods in whether Mn_3N_2 is a near hull or on the hull compound (metastable or stable). Therefore, we propagate the mean absolute error (MAE) of ~35 meV/atom for evaluating the 0K decomposition enthalpy and near hull stability of Mn_3N_2 throughout the computational predictions provided in this work.[34] This MAE is applicable towards the evaluation of solid phase reaction energetics, such as the decomposition of compounds into other compounds, etc., and is of comparable magnitude to the experimental

uncertainty (~ 22 meV/atom for a binary compound) in evaluating these enthalpies.[34] Compound free energies at finite temperatures were computed using a statistical-descriptor for inorganic crystalline solid Gibbs formation energies.[35] Crystal Orbital Hamilton Populations (COHP) used in analyzing the bonding and electronic structure were obtained using the LOBSTER code.[36]

RESULTS

The structure of manganese nitride, Mn_3N_2, adopts a body-centered tetragonal unit cell and is pictured in **Figure 1.** Nitrogen atoms occupy two-thirds of the octahedral sites allowing for two distinct manganese atom locations. One manganese atom is linearly coordinated to the interstitial nitrogens, while the other atom is coordinated in a square pyramidal fashion to five nitrogen atoms. The unit cell parameters of synthesized Mn_3N_2 are within uncertainty (evaluated from PXRD) of those found in the literature; a = 2.974 Å and c = 12.126 Å ($I4/mmm$).[16]

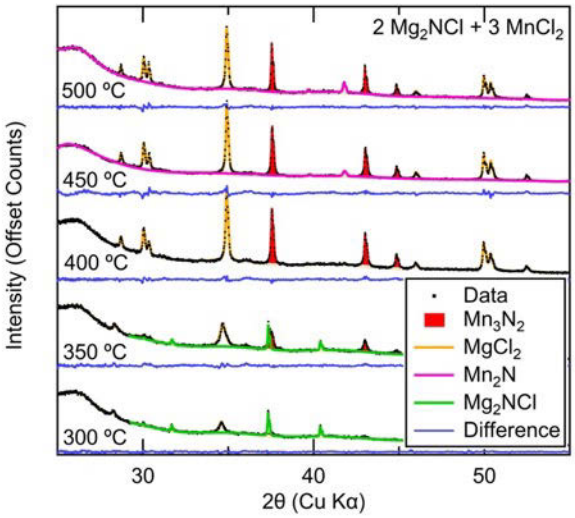

Figure 2: PXRD data of the products from 2 Mg_2NCl + 3 $MnCl_2$ at different muffle furnace set points (12 h dwell times, actual reaction temperatures ~20-40 °C lower). The data and fitted curves are shown with a constant offset for clarity. Data are shown as black dots; difference between the data and calculated in blue lines. Contributions from each phase (determined via Rietveld method) are displayed as colored lines except for the Mn_3N_2 compound, which is shown as a solid red fill. The data show a decrease in diffraction intensity from the reactants with increasing temperature, concomitant with an increase in Mn_3N_2 and $MgCl_2$ phases. At higher set points (450 °C to 500 °C), Mn_2N is observed while Mn_3N_2 decreases in intensity.

Stoichiometric control of the reaction of 2 Mg_2NCl + 3 $MnCl_2$ ⟶ Mn_3N_2 + 4$MgCl_2$ is optimized at muffle furnace set points of 400 °C. PXRD patterns of the reaction products over a temperature set point range from 300 °C to 500 °C are shown in **Figure 2**, and the respective quantitative phase analysis is tabulated in **Table SI**. At lower temperatures, solid-solution $Mg_xMn_{1-x}Cl_2$ phases are also observed. Set points above 400 °C lead to the decomposition of Mn_3N_2 to the nitrogen deficient phase, Mn_2N. Similar trends are noted for the reaction Mg_3N_2 + 3 $MnCl_2$ → Mn_3N_2 + 3 $MgCl_2$ (**Figure S1**).

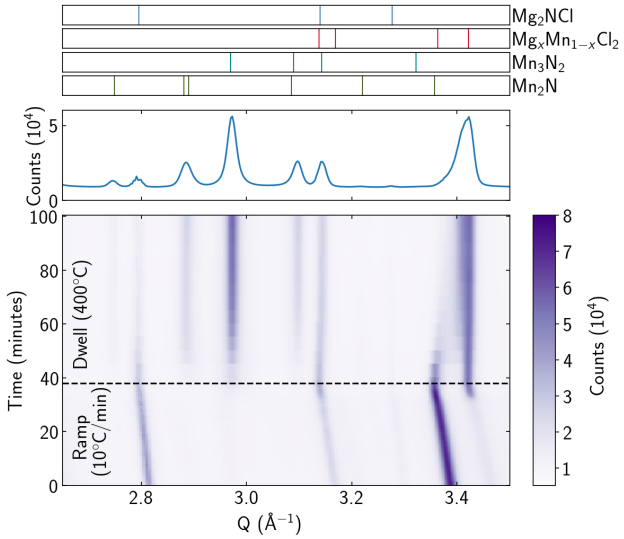

Figure 3. False color image of *in situ* PXRD data of 2Mg_2NCl + 3$MnCl_2$, ramped from room temperature to 400 °C at a rate of 10 °C/min, showing a focused Q range. The horizontal dashed line denotes the time at which 400 °C is reached and maintained. We estimate the error in temperature at the sample is ±1 °C. Tick marks show peak positions for phases in the final scan shown at top. The full Q range is shown in **Figure S2**.

In situ PXRD patterns reveal direct conversion of Mg_2NCl and $MnCl_2$ to $MgCl_2$ and Mn_3N_2, with a trace quantity of Mn_2N detected at higher temperatures after isothermal dwell (**Figure 3**). No other crystalline intermediates are detected. In addition to the observation of thermal expansion during heating, the peaks from Mg_2NCl decrease in intensity over time, while Mn_3N_2 forms after 35 minutes (T = 370 °C). As the reaction proceeds, the ($2\bar{1}$ 0) peak of

$Mg_xMn_{1-x}Cl_2$ decreases in Q (due to contraction along the a axis) and decreases in intensity, while the $(10\overline{8})$ peak grows in intensity, suggesting Mg substitution at Mn sites. Mn_2N formation is observable at 400 °C (38 min). These data reveal a narrow temperature window in which Mg_2NCl is a kinetically-competent precursor for formation of Mn_3N_2, but above which formation of Mn_2N competes and Mn_3N_2 decomposes (**Figure S4**). Within this window however, Mn_2N formation is not detectable by *ex situ* PXRD, even at reaction dwell times as long as 1 month (**Figure S3**).

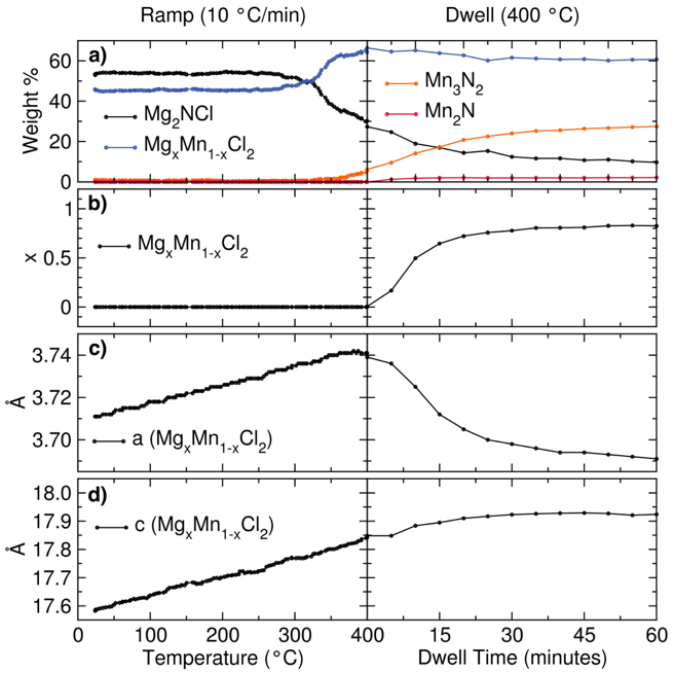

Figure 4. Summary of Rietveld analysis results from the *in situ* PXRD experiment of $2Mg_2NCl + 3MnCl_2$, ramped from room temperature to 400 °C at a rate of 10 °C/min (**Figure 3).** (a) The phase fraction of Mg_2NCl decreases as manganese nitride phases form, which corresponds with (b) a change in occupancy and (c) a contraction in the *a* lattice parameter of $Mg_xMn_{1-x}Cl_2$. (d) The *c* lattice parameter of $Mg_xMn_{1-x}Cl_2$ expands slightly.

Solid-solution behavior of the $MnCl_2$ precursor with the $MgCl_2$ product is observed through Rietveld analysis of the *in situ* PXRD data (**Figure 4**). The increase in Mg occupancy during the dwell (**Figure 4b**) mirrors the decrease in the *a* lattice parameter for the $Mg_xMn_{1-x}Cl_2$ phase (**Figure 4c**), as the phase shifts from predominantly $MnCl_2$ (a_{298K} = 3.711 Å) to $MgCl_2$

(a_{298K} = 3.636 Å). These data are consistent with *ex situ* PXRD data under various reaction conditions (**Figures S5 and S6**). However, the *in situ* data illustrate that the rate of increasing phase fraction of Mn_3N_2 is more gradual in time than are the changes to $Mg_xMn_{1-x}Cl_2$.

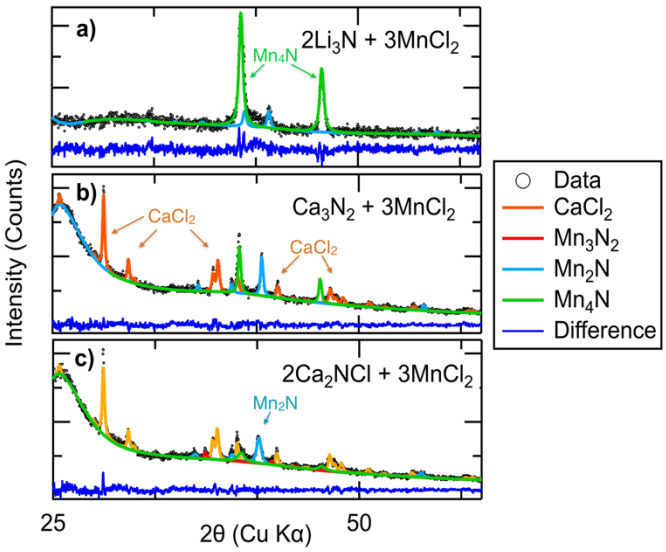

Figure 5: (a) PXRD of products from the reaction of 2 Li_3N + 3 $MnCl_2$ after self-propagation during mild heating from flame sealing the reaction ampoule. The reaction products were exposed to air, resulting in deliquescence of the LiCl to reveal only crystalline Mn_2N and Mn_4N. (b) Products from Ca_3N_2 + 3 $MnCl_2$ at 400 °C (muffle furnace set point) for 12 hours detectable by PXRD. The reaction produced $CaCl_2$ (68.58 mol%), as well as the nitrogen deficient manganese nitrides; Mn_4N (11.51 mol%) and Mn_2N (19.90 mol%). This suggests loss of nitrogen in the form of N_2(g). (c) Products from 2 Ca_2NCl + 3 $MnCl_2$ at 400 °C (muffle furnace set point) for 12 hours detectable by PXRD. Three manganese nitride compounds were formed including Mn_4N (6.76 mol%), Mn_2N (19.00 mol%), and Mn_3N_2 (2.75 mol%) along with $CaCl_2$ (71.49 mol%).

Several control reactions were attempted with other nitrogen-containing precursors in order to understand the thermochemical factors responsible for Mn_3N_2 formation. The reaction, 2 Li_3N + 3 $MnCl_2$ → Mn_3N_2 + 6 LiCl, instead produces nitrogen deficient manganese nitrides: Mn_4N and Mn_2N. The reaction mixture self-propagated under mild heat (*CAUTION!* e.g., while flame sealing; **Figure 5a**). The reaction, Ca_3N_2 + 3 $MnCl_2$ → Mn_3N_2 + 3 $CaCl_2$ also yields nitrogen-

deficient Mn-N phases, Mn_4N (11.51 mol%) and Mn_2N (19.90 mol%), as well as $CaCl_2$ (68.58 mol%; **Figure 5b**). The reaction, 2 Ca_2NCl + 3 $MnCl_2$ → Mn_3N_2 + 4 $CaCl_2$, produces a mixture of the nitrides Mn_3N_2 (2.75 mol%), Mn_4N (6.76 mol%), and Mn_2N (19.00 mol%), as well as $CaCl_2$ (71.49 mol%; **Figure 5c**).

DISCUSSION

The reactions, 2 Mg_2NCl + 3 $MnCl_2$ → Mn_3N_2 + 4 $MgCl_2$ and Mg_3N_2 + 3 $MnCl_2$ → Mn_3N_2 + 3 $MgCl_2$ proceed stoichiometrically to yield crystalline Mn_3N_2. These synthesis reactions contrast previous efforts, which rely on conditions aimed at increasing the chemical potential of nitrogen, often through pressure or highly reactive precursors.[16,20–25] The reaction here instead proceeds at relatively low temperature (~370 °C) via the interdiffusion of magnesium-based nitride precursors.

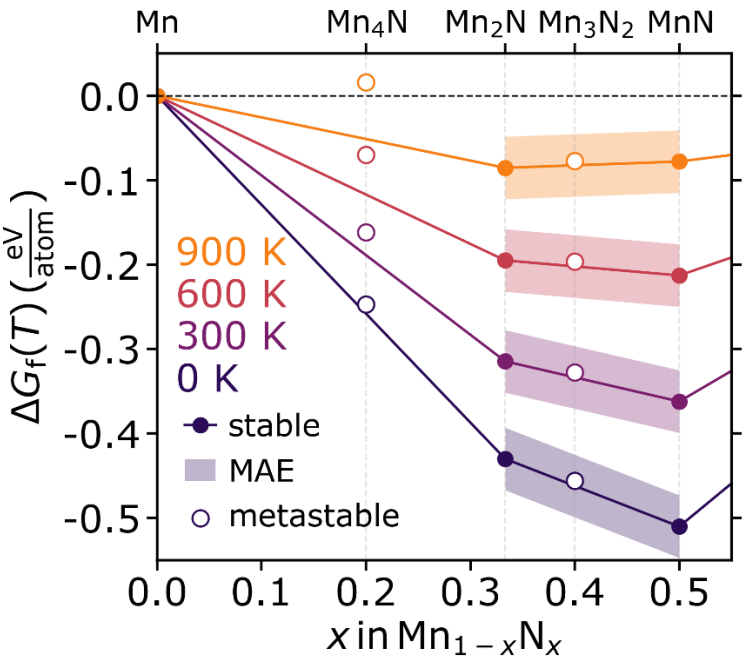

Figure 6: Convex hull phase diagram of binary manganese nitride compounds at 0 K, 300 K, 600 K, and 900 K. $\Delta G_f(T)$ is the Gibbs formation energy at the specified temperature, x is the fraction of nitrogen in the compound, and the shaded regions indicate the energetic resolution of the computational approach in evaluating the hull stability. The predicted formation energy of Mn_3N_2 relative to Mn_2N and MnN places it near the border of stability and being metastable

towards decomposition into these compounds, which is consistent with the experimentally observed challenge of readily synthesizing Mn_3N_2 using reactive nitrogen sources.

The computed convex hull phase diagram depicting the 0 K and finite temperature thermochemical stability of Mn_3N_2 illustrates the challenge towards formation of Mn_3N_2 under standard synthesis conditions (**Figure 6**). The free energy of formation falls within the ~35 meV/atom MAE uncertainty of the density functional calculations in resolving the on or near hull stability of Mn_2N_3 at 0 K,[34] and it remains within this range of uncertainty for all finite temperatures evaluated. Note that neglecting zero point energies and heat capacity contributions to the enthalpy introduces only a modest source of error, 7 meV/atom on average,[34] and that the MAE of the finite temperature predictions using the statistical-descriptor for evaluating free energies is of similar magnitude as the uncertainty in the DFT methods, ~40 meV/atom.[35] From **Figure 6**, we can see that if the Mn_3N_2 phase decomposes to release N_2 as an expected kinetic product in vacuum, Mn_2N should be observed, as consistent with our observations for reactions performed above 400 °C (**Figure S4**).

The role of controlled interdiffusion is substantiated by the observation of the solid-solution behavior of $Mg_xMn_{1-x}Cl_2$. $MgCl_2$ and $MnCl_2$ are isostructural and the ionic size of Mg^{2+} and Mn^{2+} are highly similar, thus the solubility (enthalpy of mixing) between these two compounds is high (low) and they are thermodynamically miscible at the moderate temperatures employed in our metathesis synthesis reactions.[37,38] Rietveld analysis of PXRD data shown in **Figure 2** permits extraction of the unit cell parameters and metal site occupancy of the $(Mg/Mn)Cl_2$ phases, which generally agrees with the data collected *in situ* (summarized in **Figure S5** and **Figure S6**). The reaction product, $Mg_xMn_{1-x}Cl_2$ converges to $MgCl_2$ (a = 3.636 Å and c = 17.666 Å)[39] as temperature increases. Given the X-ray scattering contrast between Mg (Z = 12) and Mn (Z = 25), the refined occupancy of Mg^{2+} in the salt phase also increases as a function of temperature, converging to complete Mg^{2+} occupancy as a function of temperature and time with both precursors. Effectively, the salt solution affords the ions in the reaction mixture a transient place for diffusion to occur.

Analysis of the *in situ* PXRD data shows that the $MgCl_2$ forms faster than Mn_3N_2 can be detected. This is reflected in the different slopes of **Figure 4a** during the isothermal dwell at 400 °C. This transient stoichiometric imbalance strongly hints at the presence of an amorphous

phase generated in this low-temperature reaction. As a control, a known mass fraction of crystalline Si (< 2 wt% amorphous component) was added into the mixture of reaction products after the reaction was completed but before collecting PXRD data. Quantitative phase analysis relative to the known amount of Si reveals the presence of an amorphous component in the mixture (**Figure S3**). A comparison with the initial composition suggests that the amorphous component is predominantly composed of $MgCl_2$. The formation of an amorphous precursor during a kinetically-controlled reaction has previously been observed by us in solid-state metathesis reactions[12] and warrants further future study, as it may provide access to the most metastable polymorphs that can be synthesized.[40] We do not detect the exact intermediate containing the nitrogen, though we infer that it must contain Mn and N, otherwise the nitrogen would escape the solid product as N_2(g). We do not see evidence for solid-solution behavior as $Mg_{3-x}Mn_xN_2$; therefore, we must speculate the Mn_3N_2 forms by itself a second phase.

Solid-solution behavior is not observed between LiCl and $MnCl_2$ or between $CaCl_2$ and $MnCl_2$. In those cases, the cation size differences are likely large enough to increase mixing enthalpies, and the phases have distinct structures; such a structural discontinuity precludes facile pathways for itinerant ions. This factor may contribute to the observation of nitrogen-poor Mn_4N phase formation in the corresponding reactions, rather than stoichiometric reaction. Without a pathway for ion intercalation, it is possible that random assortment of ions within the reaction mixture occurs, and the formation of nitrogen gas can readily take place. Upon formation of N_2, the chemical activity of nitrogen is reduced to ineffective levels.

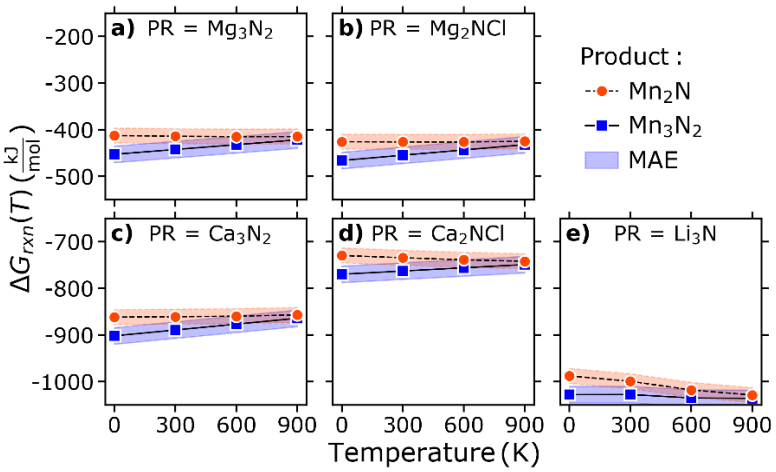

Figure 7. Calculated reaction free energies of nitride metathesis reactions (PR denotes the precursor for each reaction, full reactions listed in Table SIII). Mn_3N_2 formation is

thermodynamically favored over decomposition to subnitride kinetic products (i.e., Mn_3N_2 $\rightarrow$1.5 Mn_2N + 0.25 N_2) below 900 K. Above 1000 K, decomposition to the elements is favored (not shown). Reaction of $MnCl_2$ with Mg-based precursors produces less exergonic reactions than with Ca- and Li-based precursors. The uncertainty in the computational precision of resolving the (meta-)stability of Mn_3N_2 is propagated into the reaction free energy calculations and indicated by the shaded regions.

Thermochemistry provides a counterintuitive perspective on the experimental observations, in that the least exergonic reactions are those which yield the targeted phase. Free energies of reaction derived from first-principles calculations (**Figure 7**), illustrate that the Mg_2NCl and Mg_3N_2 sourced reactions are about half as exergonic as the analogous Ca_2NCl and Ca_3N_2 reactions, as loosely attributable to the lower $\Delta G_f(T)$ of the $CaCl_2$ relative to $MgCl_2$, even at typical synthesis conditions (T = 600-900 K). One possible explanation is that the formation of the respective salts in these reactions generate enough heat locally that even if Mn_3N_2 forms, it will decompose into the reduced nitrides, metal, and nitrogen gas, as previously observed.[8] Crystal Orbital Hamilton Population (COHP)[41] calculations show that Mg_3N_2 is more covalent than Ca_3N_2 (**Figure S7**), which may also kinetically inhibit N_2 formation by having both a higher Mg-N bond dissociation energy and bond directionality, inhibiting off-stoichiometry from the liberation and transport of ions allowing the Mg_3N_2 to produce the targeted phase while Ca_3N_2 produces subnitrides. Alternatively, for highly exergonic reactions (e.g., with Ca_3N_2, Ca_2NCl, and Li_3N), the systems appear to form compounds that would produce the fastest change in free energy ($\Delta G/\Delta t$), as observed in thin film metallurgical junctions;[42,43] the rapid formation of $N_2(g)$ as a kinetic product does not require a concerted nucleation and growth process. This may be why Mn_2N is is observed instead of forming a more thermodynamically favorable MnN phase. However, this rapid free energy change refers to the local reaction zone, as rapid heating of 2 Mg_2NCl + 3 $MnCl_2$ still produces Mn_3N_2 (**Figure S8**).

CONCLUSION

Manganese nitride (Mn_3N_2) is formed stoichiometrically *via* a kinetically-controlled solid-state metathesis reaction between 2 Mg_2NCl and 3 $MnCl_2$ and between Mg_3N_2 and 3 $MnCl_2$. The reaction proceeds without loss of nitrogen and yields crystalline products. The

controlled reaction is afforded by a low heat of reaction (< 400 kJ mol^{-1}) and the solid solution between the reactants and products ($MgCl_2$ and $MnCl_2$) enables the reaction to proceed at a relatively low temperature. Free energy calculations suggest Mn_3N_2 is thermodynamically stable up to 900 K, although experiments show N_2 formation competes as the reaction temperature increases above ~380 °C. Control reactions using other nitride binaries reveal that a small free energy change in time ($\Delta G/\Delta t$) is required in synthesizing materials that decompose at elevated temperatures, such as Mn_3N_2. Using precursors with a reasonably high nitrogen bond dissociation energy also appears to prevent loss of nitrogen to N_2 during the reaction (e.g., Mg_3N_2 vs. Ca_3N_2). The use of kinetically-controlled reactions to prescribe synthesis reactions for nominally refractory solids (e.g., nitrides) will continue to increase the diversity of nitride-based materials available for study.

ACKNOWLEDGMENTS

Work at Colorado State University was supported by the National Science Foundation (DMR-1653863). JRN and AMH acknowledge partial support for collaborative work from the Research Corporation for Science Advancement through a Scialog® Team Award. JRN acknowledges partial support from a Sloan Research Fellowship. NRS, CJB and AMH also acknowledge support in part for this work from the "Center for the Next Generation of Materials by Design", an Energy Frontier Research Center (EFRC) funded by U.S. Department of Energy (DOE), Office of Science, Basic Energy Sciences under Contract No. DE-AC36-08GO28308 to NREL. This research used resources of the Advanced Photon Source, a U.S. Department of Energy (DOE) Office of Science User Facility operated for the DOE Office of Science by Argonne National Laboratory under Contract No. DE-AC02-06CH11357. CLR and PKT acknowledge assistance Dr. Wenqian Xu and Dr. Andrey Yakovenko (17-BM-B, APS).

REFERENCES

(1) Niewa, R.; DiSalvo, F. J. Recent Developments in Nitride Chemistry. *Chem. Mater.* **1998**, *10* (10), 2733–2752.

(2) Sun, W.; Holder, A.; Orvañanos, B.; Arca, E.; Zakutayev, A.; Lany, S.; Ceder, G. Thermodynamic Routes to Novel Metastable Nitrogen-Rich Nitrides. *Chem. Mater.* **2017**, *29* (16), 6936–6946.

(3) zur Loye, H.-C.; Houmes, J. D.; Bem, D. S. Recent Developments in Ternary Nitride

Chemistry. In *The Chemistry of Transition Metal Carbides and Nitrides*; Springer Netherlands: Dordrecht, 1996; Vol. 10, pp 154–174.

(4) Arca, E.; Lany, S.; Perkins, J. D.; Bartel, C. J.; Mangum, J.; Sun, W.; Holder, A.; Ceder, G.; Gorman, B.; Teeter, G.; et al. Redox-Mediated Stabilization in Zinc Molybdenum Nitrides Redox-Mediated Stabilization in Zinc Molybdenum Nitrides. **2018**.

(5) Sun, W.; Bartel, C.; Arca, E.; Bauers, S.; Matthews, B.; Orvañanos, B.; Chen, B.-R.; Toney, M. F.; Schelhas, L. T.; Tumas, W.; et al. A Map of the Inorganic Ternary Metal Nitrides. *Prep.* **2018**.

(6) Gillan, E. G.; Kaner, R. B. Rapid Solid-State Synthesis of Refractory Nitrides. *Inorg. Chem.* **1994**, *33* (25), 5693–5700.

(7) Hector, A. L.; Parkin, I. P. Sodium Azide as a Reagent for Solid State Metathesis Preparations of Refractory Metal Nitrides. *Polyhedron* **1995**, *14* (7), 913–917.

(8) Parkin, I. P. Solid State Metathesis Reaction for Metal Borides, Silicides, Pnictides and Chalcogenides: Ionic or Elemental Pathways. *Chem. Soc. Rev.* **1996**, *25* (3), 199.

(9) Gillan, E. G.; Kaner, R. B. Synthesis of Refractory Ceramics via Rapid Metathesis Reactions between Solid-State Precursors. *Chem. Mater.* **1996**, *8* (2), 333–343.

(10) Martinolich, A. J.; Neilson, J. R. Pyrite Formation via Kinetic Intermediates through Low-Temperature Solid-State Metathesis. *J. Am. Chem. Soc.* **2014**, *136* (44).

(11) Martinolich, A. J.; Kurzman, J. A.; Neilson, J. R. Polymorph Selectivity of Superconducting CuSe2 Through Kinetic Control of Solid-State Metathesis. *J. Am. Chem. Soc.* **2015**, *137* (11), 3827–3833.

(12) Martinolich, A. J.; Kurzman, J. A.; Neilson, J. R. Circumventing Diffusion in Kinetically Controlled Solid-State Metathesis Reactions. *J. Am. Chem. Soc.* **2016**, *138* (34), 11031–11037.

(13) Martinolich, A. J.; Neilson, J. R. Toward Reaction-by-Design: Achieving Kinetic Control of Solid State Chemistry with Metathesis. *Chem. Mater.* **2017**, *29* (2).

(14) Todd, P. K.; Neilson, J. R. Selective Formation of Yttrium Manganese Oxides through Kinetically Competent Assisted Metathesis Reactions. *J. Am. Chem. Soc.* **2019**, *141* (3), 1191–1195.

(15) Okamoto, H. Comment on Mn-N (Manganese-Nitrogen). *J. phase equilibria* **1994**, *15* (4), 451–452.

(16) Leineweber, A.; Niewa, R.; Jacobs, H.; Kockelmann, W. The Manganese Nitrides η-Mn3N2 and θ-Mn6N(5+x): Nuclear and Magnetic Structures. *J. Mater. Chem.* **2000**.

(17) Walter, C.; Menezes, P. W.; Orthmann, S.; Schuch, J.; Connor, P.; Kaiser, B.; Lerch, M.; Driess, M. A Molecular Approach to Manganese Nitride Acting as a High Performance Electrocatalyst in the Oxygen Evolution Reaction. *Angew. Chemie - Int. Ed.* **2018**.

(18) Takei, W. J.; Heikes, R. R.; Shirane, G. Magnetic Structure of Mn4N-Type Compounds. *Phys. Rev.* **1962**, *125* (6), 1893–1897.

(19) Mekata, M.; Haruna, J.; Takaki, H. Neutron Diffraction Study of Antiferromagnetic Mn2N. *J. Phys. Soc. Japan* **1968**, *25* (1), 234–238.

(20) Suzuki, K.; Kaneko, T.; Yoshida, H.; Morita, H.; Fujimori, H. Crystal Structure and Magnetic Properties of the Compound MnN. *J. Alloy. Compd.* **1995**, *224* (2), 232–236.

(21) Yang, H.; Al-Brithen, H.; Smith, A. R.; Borchers, J. A.; Cappelletti, R. L.; Vaudin, M. D. Structural and Magnetic Properties of η-Phase Manganese Nitride Films Grown by Molecular-Beam Epitaxy. *Appl. Phys. Lett.* **2001**, *78* (24), 3860–3862.

(22) Si, P. Z.; Jiang, W.; Wang, H. X.; Zhong, M.; Ge, H. L.; Chul-Jin, C.; Jung-Goo, L. The High Nitrogen Pressure Synthesis of Manganese Nitride. *Chinese Phys. Lett.* **2012**, *29* (12).

(23) Parkin, I. P.; Rowley, A. T. Formation of Transition-Metal Nitrides from the Reactions of Lithium Amides and Anhydrous Transition-Metal Chlorides. *J. Mater. Chem.* **1995**, *5* (6), 909–912.

(24) Miura, A.; Takei, T.; Kumada, N. Low-Temperature Nitridation of Manganese and Iron Oxides Using NaNH 2 Molten Salt. *Inorg. Chem.* **2013**, *52* (20), 11787–11791.

(25) Jacobs, G. K. H. Magnetische Struktur von η-Mn3N2. **1992**, *183*, 345–362.

(26) Stein, A.; Keller, S. W.; Mallouk, T. E.; Desimone, D. M.; Desrosiers, P. J.; Hughes, R. P. Turning Down the Heat : Design and Mechanism in Solid-State Synthesis. **2016**, *259* (5101), 1558–1564.

(27) Li, Y.; George, J.; Liu, X.; Dronskowski, R. Synthesis, Structure Determination and Electronic Structure of Magnesium Nitride Chloride, Mg_2NCl. *Zeitschrift für Anorg. und Allg. Chemie* **2015**, *641* (2), 266–269.

(28) Hadenfeldt, C.; Herdejürgen, H. Darstellung Und Kristallstruktur Der Calciumnitridhalogenide Ca2NCl Und Ca2NBr. *Zeitschrift für Anorg. und Allg. Chemie*

1987, *545* (2), 177–183.

(29) Toby, B. H.; Von Dreele, R. B. GSAS-II : The Genesis of a Modern Open-Source All Purpose Crystallography Software Package. *J. Appl. Crystallogr.* **2013**, *46* (2), 544–549.

(30) Kresse, G.; Furthmüller, J. Efficient Iterative Schemes for *Ab Initio* Total-Energy Calculations Using a Plane-Wave Basis Set. *Phys. Rev. B* **1996**.

(31) Kresse, G.; Joubert, D. From Ultrasoft Pseudopotentials to the Projector Augmented-Wave Method. *Phys. Rev. B* **1999**, *59* (3), 1758–1775.

(32) Perdew, J. P.; Burke, K.; Ernzerhof, M. Generalized Gradient Approximation Made Simple. *Phys. Rev. Lett.* **1996**.

(33) Jain, A.; Ong, S. P.; Hautier, G.; Chen, W.; Richards, W. D.; Dacek, S.; Cholia, S.; Gunter, D.; Skinner, D.; Ceder, G.; et al. Commentary: The Materials Project: A Materials Genome Approach to Accelerating Materials Innovation. *APL Mater.* **2013**, *1* (1), 011002.

(34) Bartel, C. J.; Weimer, A. W.; Lany, S.; Musgrave, C. B.; Holder, A. M. The Role of Decomposition Reactions in Assessing First-Principles Predictions of Solid Stability. *npj Comput. Mater.* **2019**, *5* (1), 4.

(35) Bartel, C. J.; Millican, S. L.; Deml, A. M.; Rumptz, J. R.; Tumas, W.; Weimer, A. W.; Lany, S.; Stevanović, V.; Musgrave, C. B.; Holder, A. M. Physical Descriptor for the Gibbs Energy of Inorganic Crystalline Solids and Temperature-Dependent Materials Chemistry. *Nat. Commun.* **2018**, *9* (1), 4168.

(36) Maintz, S.; Deringer, V. L.; Tchougréeff, A. L.; Dronskowski, R. LOBSTER: A Tool to Extract Chemical Bonding from Plane-Wave Based DFT. *J. Comput. Chem.* **2016**, *37* (11), 1030–1035.

(37) Robelin, C.; Chartrand, P.; Pelton, A. D. Thermodynamic Evaluation and Optimization of the (NaCl+KCl+MgCl2+CaCl2+MnCl2+FeCl2+CoCl2+NiCl2) System. *J. Chem. Thermodyn.* **2004**, *36* (9), 809–828.

(38) Korzhukov, N. G.; Ozerova, M. I.; Khomyakov, K. G.; Onikienko, L. D. Melting Diagram of the System MgCl2-MnCl2. *Vestn. Mosk. Univ., Ser. 2* **1695**, *21* (4), 59–60.

(39) Partin, D. E.; O'Keeffe, M. The Structures and Crystal Chemistry of Magnesium Chloride and Cadmium Chloride. *J. Solid State Chem.* **1991**, *95* (1), 176–183.

(40) Aykol, M.; Dwaraknath, S. S.; Sun, W.; Persson, K. A. Thermodynamic Limit for Synthesis of Metastable Inorganic Materials. *Sci. Adv.* **2018**, *4* (4), 1–8.

(41) Dronskowski, R.; Bloechl, P. E. Crystal Orbital Hamilton Populations (COHP): Energy-Resolved Visualization of Chemical Bonding in Solids Based on Density-Functional Calculations. *J. Phys. Chem.* **1993**, *97* (33), 8617–8624.

(42) Walser, R. M.; Bené, R. W. First Phase Nucleation in Silicon–Transition-Metal Planar Interfaces. *Appl. Phys. Lett.* **1976**, *28* (10), 624.

(43) Bené, R. W. A Kinetic Model for Solid-state Silicide Nucleation. *J. Appl. Phys.* **1987**, *61* (5), 1826–1833.

TOC Graphic:

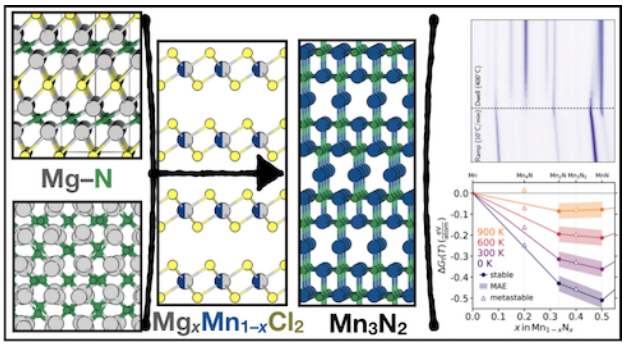
Mg–N
$Mg_xMn_{1-x}Cl_2$
Mn_3N_2
900 K
600 K
300 K
0 K
stable
MAE
metastable
0.0
-0.1
-0.2
-0.3
-0.4
-0.5
0.0 0.1 0.2 0.3 0.4 0.5